NASA TECHNICAL NOTE

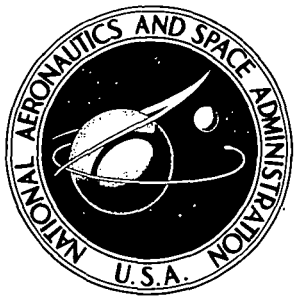

NASA TN D-7213

NASA TN D-7213

THREE-DIMENSIONAL ELASTIC STRESS AND DISPLACEMENT ANALYSIS OF TENSILE FRACTURE SPECIMENS CONTAINING CRACKS

by John P. Gyekenyesi, Alexander Mendelson, and Jon Kring

Lewis Research Center
and
U.S. Army Air Mobility R&D Laboratory
Cleveland, Ohio 44135

NATIONAL AERONAUTICS AND SPACE ADMINISTRATION • WASHINGTON, D. C. • APRIL 1973

Page Intentionally Left Blank

1. Report No. NASA TN D-7213	2. Government Accession No.	3. Recipient's Catalog No.
4. Title and Subtitle THREE-DIMENSIONAL ELASTIC STRESS AND DISPLACEMENT ANALYSIS OF TENSILE FRACTURE SPECIMENS CONTAINING CRACKS		5. Report Date April 1973 6. Performing Organization Code
7. Author(s) John P. Gyekenyesi, Alexander Mendelson, and Jon Kring		8. Performing Organization Report No. E-7170 10. Work Unit No. 501-21
9. Performing Organization Name and Address NASA Lewis Research Center and U.S. Army Air Mobility R&D Laboratory Cleveland, Ohio 44135		11. Contract or Grant No. 13. Type of Report and Period Covered Technical Note
12. Sponsoring Agency Name and Address National Aeronautics and Space Administration Washington, D.C. 20546		14. Sponsoring Agency Code
15. Supplementary Notes		

16. Abstract

A seminumerical method is presented for three-dimensional elastic analysis of finite geometry solids with traction-free cracks. Stress and displacement distributions are calculated for two rectangular bars which are loaded by a uniform surface stress distribution. The first bar contains a through-thickness central crack while the second bar has double-edge cracks. Stress intensity factors K_I for both configurations are presented.

17. Key Words (Suggested by Author(s))	18. Distribution Statement
Three-dimensional elasticity; Fracture mechanics; Central crack; Double-edge crack; Stress intensity factor; Displacements; Stresses	Unclassified - unlimited

19. Security Classif. (of this report)	20. Security Classif. (of this page)	21. No. of Pages	22. Price*
Unclassified	Unclassified	41	$3.00

* For sale by the National Technical Information Service, Springfield, Virginia 22151

Page Intentionally Left Blank

Page Intentionally Left Blank

THREE-DIMENSIONAL ELASTIC STRESS AND DISPLACEMENT ANALYSIS OF TENSILE FRACTURE SPECIMENS CONTAINING CRACKS

by John P. Gyekenyesi, Alexander Mendelson, and Jon Kring

Lewis Research Center

SUMMARY

The line method of analysis is applied to the Navier-Cauchy equations of elastic equilibrium to calculate the displacement distributions in frequently used tensile fracture specimens. The application of this method to these equations leads to coupled sets of simultaneous ordinary differential equations whose solutions are obtained along sets of lines in a discretized region. When decoupling the equations and their boundary conditions is not possible, the use of a successive approximation procedure permits the analytical solution of the resulting ordinary differential equations. The results obtained show a considerable potential for using this method in the three-dimensional analysis of finite geometry solids and suggest a possible extension of this technique to nonlinear material behavior.

INTRODUCTION

Considerable progress has been made in recent years in the stress analysis of bodies containing flaws or cracks. However, most of the work on this subject has been based on the plane theory of elasticity (ref. 1). For a fracture specimen of finite geometry the stress and displacement fields are highly three-dimensional. Hence, solutions of the general elasticity field equations must be obtained when more reliable results are needed.

Because of the geometric singularity associated with any crack type problem, there is almost no possibility of a simple closed form type of solution. For this reason, three-dimensional elastic solutions have been obtained only for a restricted class of problems (refs. 2 to 4). Recently, with the availability of large digital computers, a variety of numerical methods appeared in the literature; however, most of these methods have yielded only partial results. Among these approximate methods are the finite

difference (ref. 5), the direct potential (ref. 6), the eigenfunction expansion (ref. 7), and the line method of analysis (ref. 8). Of all these solution techniques, the line method of analysis appears to yield the most complete and accurate results for three-dimensional elasticity problems.

Although the concept of the line method for solving partial differential equations is not new (ref. 9), its application in the past has been limited to simple examples (ref. 10). The line method lies midway between completely analytical and discrete methods. The basis of this technique is the substitution of finite differences for the derivatives with respect to all the independent variables except one for which the derivatives are retained. This approach replaces a given partial differential equation with a system of simultaneous ordinary differential equations whose solutions can then be obtained in closed form. These equations describe the dependent variable along lines which are parallel to the coordinate in whose direction the derivatives were retained. Application of the line method is most useful when the resulting ordinary differential equations are linear and have constant coefficients.

An inherent advantage of the line method over other numerical methods is that good results are obtained from the use of relatively coarse grids. This use of a coarse grid is permissible because parts of the solutions are obtained in terms of continuous functions. Additional accuracy in normal stress distributions is derived from the fact that they are expressed as first-order derivatives of the displacements and these derivatives can be analytically evaluated. Inherently inaccurate numerical differentiation is required only for evaluating the shear stresses, but this presents no important loss of accuracy since they are an order of magnitude smaller than the normal stresses. For problems with geometric singularities, additional accuracy is derived from using a displacement formulation since the resulting deformations are not singular.

It is the purpose of this report to present a simple and systematic approach to the elastic analysis of three-dimensional, finite geometry solids containing traction-free central or edge cracks. The need for these specific solutions has existed for a number of years in fracture toughness testing, and several attempts in the past have failed to arrive at meaningful results (refs. 11 and unpublished data by G. C. Sih and R. J. Hartranft of Lehigh University (NASA Grant NGR-39-007-025)). Problems that are most conveniently described in rectangular Cartesian coordinates are discussed herein while circular geometry solids will be treated in a subsequent report.

SYMBOLS

A_{ij} $i = j = 2$, partitioned submatrices of $e^{A\tilde{x}}$

$A(x)$ coefficient matrix of first-order, x-directional differential equations

$2a$	crack width
B_i	partitioned particular integrals, $i = 1, 2, 3, 4$
$2b$	bar width
E	Young's modulus of elasticity
e	dilatation or natural logarithm base
G	shear modulus of elasticity
h_x, h_y, h_z	increments along Cartesian coordinate axes
I	identity matrix
K_I	stress intensity factor for opening mode
K_x, K_y, K_z	coefficient matrices of second-order differential equations
$2L$	bar length
l	number of lines in x-direction
m	number of lines in y-direction
NX, NY, NZ	number of lines in a given plane
n	number of lines in z-direction
R	distance from crack edge
$r(x)$	coupling vector for x-directional second-order differential equations
$s(y)$	coupling vector for y-directional second-order differential equations
$2t$	bar thickness
$t(z)$	coupling vector for z-directional second-order differential equations
u	x-directional displacement
v	y-directional displacement
w	z-directional displacement
x, y, z	rectangular Cartesian coordinates
λ	Lame's constant
η	variable of integration
ν	Poisson's ratio
$\sigma_x, \sigma_y, \sigma_z, \sigma_{xy}, \sigma_{zx}, \sigma_{yz}$	components of the stress tensor in Cartesian coordinates

∇^2 Laplacian in Cartesian coordinates

Symbols used in the appendixes are defined there when they are introduced.

REDUCTION OF THE NAVIER-CAUCHY EQUATIONS TO SYSTEMS OF ORDINARY DIFFERENTIAL EQUATIONS

Within the framework of linearized elasticity theory, the equations of elastic equilibrium in terms of displacements are

$$(\lambda + G)\frac{\partial e}{\partial x} + G\nabla^2 u = 0 \tag{1}$$

$$(\lambda + G)\frac{\partial e}{\partial y} + G\nabla^2 v = 0 \tag{2}$$

$$(\lambda + G)\frac{\partial e}{\partial z} + G\nabla^2 w = 0 \tag{3}$$

where the body forces are assumed to be zero and the dilatation is

$$e = \frac{\partial u}{\partial x} + \frac{\partial v}{\partial y} + \frac{\partial w}{\partial z} \tag{4}$$

The stress-displacement relations can be written as

$$\sigma_x = \frac{E}{(1 + \nu)(1 - 2\nu)}\left[(1 - \nu)\frac{\partial u}{\partial x} + \nu\left(\frac{\partial v}{\partial y} + \frac{\partial w}{\partial z}\right)\right] \tag{5}$$

$$\sigma_y = \frac{E}{(1 + \nu)(1 - 2\nu)}\left[(1 - \nu)\frac{\partial v}{\partial y} + \nu\left(\frac{\partial w}{\partial z} + \frac{\partial u}{\partial x}\right)\right] \tag{6}$$

$$\sigma_z = \frac{E}{(1 + \nu)(1 - 2\nu)}\left[(1 - \nu)\frac{\partial w}{\partial z} + \nu\left(\frac{\partial u}{\partial x} + \frac{\partial v}{\partial y}\right)\right] \tag{7}$$

$$\sigma_{xy} = \frac{E}{2(1 + \nu)}\left(\frac{\partial v}{\partial x} + \frac{\partial u}{\partial y}\right) \tag{8}$$

$$\sigma_{zx} = \frac{E}{2(1+\nu)}\left(\frac{\partial u}{\partial z} + \frac{\partial w}{\partial x}\right) \tag{9}$$

$$\sigma_{yz} = \frac{E}{2(1+\nu)}\left(\frac{\partial w}{\partial y} + \frac{\partial v}{\partial z}\right) \tag{10}$$

For a finite geometry solid with rectangular boundaries. we construct three sets of parallel lines (fig. 1(a)). Each set of lines is parallel to one of the coordinate axes and thus perpendicular to the corresponding coordinate plane. An approximate solution of equation (1) can then be obtained by developing solutions of ordinary differential equations along the x-directional lines. As seen in the figure, there are a total of $\ell = NY \times NZ$ such lines where NY is the number of lines along the y-direction and NZ is the number of lines along the x-direction in a given plane, respectively. We define the displacements along these lines as $u_1, u_2, \ldots, u_\ell$. The derivatives of the y-directional displacements on these lines with respect to y are defined as $\dot{v}|_1, \dot{v}|_2, \ldots, \dot{v}|_\ell$, and the derivatives of the z-directional displacements with respect to z are defined as $\dot{w}|_1, \dot{w}|_2, \ldots, \dot{w}|_\ell$. These displacements and derivatives can then be regarded as functions of x only since they are variables on x-directional lines. When these definitions are used, the ordinary differential equation along a generic line ij (a double subscript is used here for simplicity of writing) in figure 1(b) may be written as

$$\frac{d^2u_{ij}}{dx^2} + \frac{(1-2\nu)}{2(1-\nu)}\left[-\left(\frac{2}{h_y^2} + \frac{2}{h_z^2}\right)u_{ij} + \frac{1}{h_y^2}(u_{i+1,j} + u_{i-1,j}) + \frac{1}{h_z^2}(u_{i,j+1} + u_{i,j-1})\right] + \frac{f_{ij}(x)}{2(1-\nu)} = 0 \tag{11}$$

where

$$f_{ij}(x) = \left.\frac{d\dot{v}}{dx}\right|_{ij} + \left.\frac{d\dot{w}}{dx}\right|_{ij} \tag{12}$$

$$\dot{v} = \frac{dv}{dy}$$

and

$$\dot{w} = \frac{dw}{dz}$$

Similar differential equations are obtained along the other x-directional lines. Since each equation has the terms of the displacements on the surrounding lines, these equations constitute a system of ordinary differential equations for the displacements u_1, u_2, . . ., u_l.

It is convenient to nondimensionalize equations (11) and (12) with respect to some characteristic dimension of the problem. Hence, we introduce the following variables:

$$\left.\begin{aligned} \tilde{u} &= \frac{u}{a} & \tilde{x} &= \frac{x}{a} & \tilde{h}_x &= \frac{h_x}{a} \\ \tilde{v} &= \frac{v}{a} & \tilde{y} &= \frac{y}{a} & \tilde{h}_y &= \frac{h_y}{a} \\ \tilde{w} &= \frac{w}{a} & \tilde{z} &= \frac{z}{a} & \tilde{h}_z &= \frac{h_z}{a} \end{aligned}\right\} \tag{13}$$

where 2(a) is the crack width. In matrix notation, the differential equations along the x-directional lines of figure 1(a) can be written as

$$\underset{l\times 1}{d^2\tilde{u}/d\tilde{x}^2} = \underset{l\times l}{K_x}\ \underset{l\times 1}{\tilde{u}} + \underset{l\times 1}{r(\tilde{x})} \tag{14}$$

In a similar manner, to solve equations (2) and (3) ordinary differential equations are constructed along the y- and z-directional lines, respectively. These equations are also expressed in an analogous form to equation (14); they are

$$\underset{m\times 1}{d^2\tilde{v}/d\tilde{y}^2} = \underset{m\times m}{K_y}\ \underset{m\times 1}{\tilde{v}} + \underset{m\times 1}{s(\tilde{y})} \tag{15}$$

$$\underset{n\times 1}{d^2\tilde{w}/d\tilde{z}^2} = \underset{n\times n}{K_z}\ \underset{n\times 1}{\tilde{w}} + \underset{n\times 1}{t(\tilde{z})} \tag{16}$$

An inspection of these equations shows that they are linear, second-order, ordinary differential equations with constant coefficients. The coupling terms in each set of differential equations are grouped into the vectors $r(\tilde{x})$, $s(\tilde{y})$, and $t(\tilde{z})$, which are the nonhomogeneous terms in equations (14), (15), and (16). The elements of the coefficient matrices are functions of the coordinate increments and Poisson's ratio only. Since the sum of the elements in any given row of the three coefficient matrices is zero, they are all singular.

Noting that a second-order differential equation can satisfy only a total of two boundary conditions and since three-dimensional elasticity problems have three boundary conditions at every point of the bounding surface, some of the boundary data must be incorporated into the surface line differential equations. Hence, conditions of normal stress and displacement are enforced through the constants of the homogeneous solutions while shear stress boundary data must be incorporated into the differential equations of the surface lines. The application of the specified shear conditions permits the use of central difference approximations when surface line differential equations are constructed. The details of constructing these equations are found in reference 8.

SOLUTION OF THE SYSTEMS OF ORDINARY DIFFERENTIAL EQUATIONS

Appendix A shows the details of a solution technique for the type of simultaneous ordinary differential equations given in equation (14). This solution technique yields the following solution vector for the x-directional displacements:

$$\underset{l\times 1}{\tilde{u}(\tilde{x})} = \underset{l\times l}{A_{11}(\tilde{x})}\left[\underset{l\times 1}{\tilde{u}(0)} + \underset{l\times 1}{B_1(\tilde{x})}\right] + \underset{l\times l}{A_{12}(\tilde{x})}\left[\underset{l\times 1}{\tilde{\tilde{u}}(0)} + \underset{l\times 1}{B_2(\tilde{x})}\right] \tag{17}$$

where $A_{11}(\tilde{x})$ and $A_{12}(\tilde{x})$ are the matrix functions

$$A_{11}(\tilde{x}) = \cosh K_x^{1/2}\tilde{x} \tag{18}$$

$$A_{12}(\tilde{x}) = K_x^{-1/2} \sinh K_x^{1/2}\tilde{x} \tag{19}$$

The matrix $K_x^{1/2}$ is defined as a matrix whose square is equal to K_x. Vectors $\tilde{u}(0)$ and $\tilde{\tilde{u}}(0)$ are initial value vectors whose evaluation from given boundary conditions is discussed in appendix B. Vectors $B_1(\tilde{x})$ and $B_2(\tilde{x})$, which represent particular solutions of equations (14), are given by

$$\underset{l\times 1}{B_1(\tilde{x})} = -\int_0^{\tilde{x}} \underset{l\times l}{A_{12}(\eta)}\,\underset{l\times 1}{r(\eta)}\, d\eta \tag{20}$$

$$\underset{l\times 1}{B_2(\tilde{x})} = \int_0^{\tilde{x}} \underset{l\times l}{A_{11}(\eta)}\,\underset{l\times 1}{r(\eta)}\, d\eta \tag{21}$$

Differentiating equation (17) with respect to $\tilde{x}$ yields

$$\underset{l\times 1}{\dot{\tilde{u}}(\tilde{x})} = \underset{l\times l}{K_x}\ \underset{l\times l}{A_{12}(\tilde{x})}\left[\underset{l\times 1}{\tilde{u}(0)} + \underset{l\times 1}{B_1(\tilde{x})}\right] + \underset{l\times l}{A_{11}(\tilde{x})}\left[\underset{l\times 1}{\dot{\tilde{u}}(0)} + \underset{l\times 1}{B_2(\tilde{x})}\right] \tag{22}$$

Similar solution vectors can be constructed for equations (15) and (16) involving the y- and z-directional displacements, respectively. Since $r(\eta)$ in equations (20) and (21) is unknown, the solution of the problem is begun by assuming values for $d\tilde{v}/d\tilde{x}$, $d\dot{\tilde{v}}/d\tilde{x}$, $d\tilde{w}/d\tilde{x}$, and $d\dot{\tilde{w}}/d\tilde{x}$ along the x-directional lines. Using zero values for these required quantities is a good place to start. Then equations (17) and (22) give the first estimate for the vectors $\tilde{u}(\tilde{x})^{(1)}$ and $\dot{\tilde{u}}(\tilde{x})^{(1)}$. It is assumed, of course, that the boundary conditions $\tilde{u}(0)$ and $\dot{\tilde{u}}(0)$ are specified or known. Using these calculated values of $\tilde{u}^{(1)}$ and $\dot{\tilde{u}}^{(1)}$ we can evaluate the vector $s(\tilde{y})^{(1)}$ where we must use similarly assumed values of $d\tilde{w}/d\tilde{y}$ and $d\dot{\tilde{w}}/dy$. Analogous equations to equations (17) and (22) give the first value of $\tilde{v}(\tilde{y})^{(1)}$ and $\dot{\tilde{v}}(\tilde{y})^{(1)}$. First values of $\tilde{w}(\tilde{z})^{(1)}$ and $\dot{\tilde{w}}(\tilde{z})^{(1)}$ can then be calculated by using the first estimates of the x- and y-directional displacements and their derivatives in the coupling vector $t(\tilde{z})^{(1)}$. At this point we return to equations (17) and (22) and calculate the second values of $\tilde{u}(\tilde{x})^{(2)}$ and $\dot{\tilde{u}}(\tilde{x})^{(2)}$ based on the first values of the y- and z-directional solutions.

If the values of $\tilde{u}(\tilde{x})^{(i)}$, $\dot{\tilde{u}}(\tilde{x})^{(i)}$, $\tilde{v}(\tilde{y})^{(i)}$, $\dot{\tilde{v}}(\tilde{y})^{(i)}$, $\tilde{w}(\tilde{z})^{(i)}$, and $\dot{\tilde{w}}(\tilde{z})^{(i)}$ converge with the repetition of this procedure, an approximate solution of a given problem is determined. In general, the convergence rate for these successive calculations is dependent on the accuracy to which the matrix functions A_{ij} can be evaluated. Equation (A13) may be used to establish this required accuracy. Sufficiently large errors in the necessary matrix functions lead to divergence in the successive approximation calculations.

Since the vector $r(\eta)$ in equations (20) and (21) involves displacements and their derivatives that are defined only at the nodes, finite difference calculus must be used in evaluating its elements. Hence, integrals $B_1(\tilde{x})$ and $B_2(\tilde{x})$ are calculated by a suitable numerical integration technique.

Once the displacement field in the bar has been calculated and the successive approximation procedure has converged, the normal stress distributions along the three sets of parallel lines can be obtained from the following equations:

$$\underset{l\times 1}{\sigma_x} = \frac{E(1-\nu)}{(1+\nu)(1-2\nu)}\ \underset{l\times 1}{(\dot{\tilde{u}})_{\substack{\text{along}\\ \text{x-lines}}}} + \frac{\nu E}{(1+\nu)(1-2\nu)}\ \underset{l\times 1}{(\dot{\tilde{v}} + \dot{\tilde{w}})_{\substack{\text{along}\\ \text{x-lines}}}} \tag{23}$$

$$\underset{m\times 1}{\sigma_y} = \frac{E(1-\nu)}{(1+\nu)(1-2\nu)} \underset{m\times 1}{(\dot{\tilde{v}})_{\substack{\text{along}\\ \text{y-lines}}}} + \frac{\nu E}{(1+\nu)(1-2\nu)} \underset{m\times 1}{(\dot{\tilde{u}} + \dot{\tilde{w}})_{\substack{\text{along}\\ \text{x-lines}}}} \tag{24}$$

$$\underset{n\times 1}{\sigma_z} = \frac{E(1-\nu)}{(1+\nu)(1-2\nu)} \underset{n\times 1}{(\tilde{w})_{\substack{\text{along}\\ \text{z-lines}}}} + \frac{\nu E}{(1+\nu)(1-2\nu)} \underset{n\times 1}{(\dot{\tilde{u}} + \dot{\tilde{v}})_{\substack{\text{along}\\ \text{x-lines}}}} \tag{25}$$

Note that the normal stress equations involve only derivatives that can be evaluated analytically. The shear stresses at each node can be calculated from equations (8) to (10) but finite difference approximations must be used for the required displacement gradients.

APPLICATION TO TENSILE FRACTURE SPECIMENS CONTAINING CRACKS

A great amount of experimental work has been done in fracture mechanics (ref. 12) through the use of crack-notched specimens. In the past, many different types of specimens have been used to determine a material's fracture toughness. The most common early specimens employed in these tests were the center-cracked and double-edge-notched bar specimens. Figures 2(a) and 7(a) show the finite rectangular bars with through-thickness, traction-free central and double-edge cracks, respectively. Because of the symmetric geometry and loading, only one-eighth of the bars has to be discretized as shown in figures 2(b) and 7(b). Inspection of the derived ordinary differential equations also shows that for any numerical computation a value of Poisson's ratio must be selected. For our work, a Poisson's ratio of 1/3 is used as shown in figures 2 to 14.

NUMERICAL RESULTS

Center-Cracked Tensile Fracture Specimen

The solution of this problem was obtained by using two different sets of lines along the coordinate axes so that the convergence of the finite difference approximations could be checked. In a given direction, uniform line spacing was used in all computations with no other restriction being placed on the selection of the grid size. The crack edge location with respect to the imposed grid was assumed to be halfway between nodes specifying normal stress and displacement boundary conditions, respectively. The successive

approximation procedure required for decoupling the three sets of ordinary differential equations was terminated when the difference between successively calculated displacements at every point was less than a preset value (10^{-6}).

Selected results of the dimensionless displacements are listed in tables I to III. The dimensionless crack opening displacement is shown in figure 3. Inspection of figures 3(a) and (b) shows that the grids of lines have been sufficiently refined when the results of the 48 by 96 by 128 grid were calculated. Figure 3(a) also contains the results of the plane elasticity solutions obtained by Mendelson, Gross, and Srawley (ref. 13). It is noteworthy that the results correspond to elliptical crack profiles in all cases. The plane stress solution gives the highest crack opening displacement while the plane strain solution is very close to the results obtained at the center of the bar.

The dimensionless normal stress distributions in the crack plane are shown in figures 4 to 6 as a function of both the $\tilde{x}$- and $\tilde{z}$-coordinates. The results in these figures clearly indicate the singular nature of the normal stresses near the crack edge. As expected, the stress normal to the crack plane increases most rapidly near the crack front. A plot of these stresses in the $\tilde{z}$-direction also indicates a central region of uniform stress and a boundary layer through which the stresses decrease to the surface values. These same results show that as $\tilde{x}$ increases the stress field approaches a uniaxial state of stress which indicates that the cause of a triaxial stress field in the bar is the through-thickness central crack.

Double-Edge Crack Tensile Fracture Specimen

Selected results for the problem of figure 7(a) are presented in tables IV to VI and figures 8 to 11. These results were also obtained with two different sets of lines along the coordinate axes which were identical to the two sets used for the central crack problem. The dimensionless crack opening displacements are plotted in figure 8. Comparing figures 8(a) and (b) shows that the finite difference approximations have sufficiently converged when the results of the finer grid were calculated. Contrary to the central crack problem, the crack opening displacements in figure 8 are independent of the $\tilde{z}$-coordinate. Similar results were obtained by Cruse and Van Buren (ref. 6) for the single-edge-crack bar specimen.

The dimensionless normal stress distributions in the crack plane are shown in figures 9 to 11 as a function of both the $\tilde{x}$- and $\tilde{z}$-coordinates. Their singular nature near the crack edge is evident from the distributions shown in these figures. A plot of these stresses in the thickness direction also shows a central region of uniform stress and a boundary layer through which the stresses decrease to the surface values. Tables IV to VI contain selected results of the dimensionless displacement distributions.

STRESS INTENSITY FACTOR

It is customary in fracture mechanics to describe the plane elasticity crack opening displacement as a superposition of three basic deformation modes (ref. 1). Since the problems shown in figures 2(a) and 7(a) have geometric symmetry and are symmetrically loaded, only the opening mode of crack displacement is obtained. In terms of the stress intensity factor for the opening mode K_I, the plane elasiticity crack displacements near the crack tip are given by (ref. 1)

$$v\big|_{y=0} = \frac{2(1-\nu)}{G} K_I \sqrt{\frac{R}{2\pi}} \qquad \text{plane strain} \tag{26}$$

$$v\big|_{y=0} = \frac{2}{(1+\nu)G} K_I \sqrt{\frac{R}{2\pi}} \qquad \text{plane stress} \tag{27}$$

Since three-dimensional problems are neither in a state of plane strain nor in a state of plane stress, the definition of a stress intensity factor for these problems must be first established. Note that by definition the plane stress and plane strain stress intensity factors are equal while the displacements are approximately 12.5 percent different for $\nu = 1/3$. Since the results indicate that most of the bar in the thickness direction is approximately in a state of plane strain, equation (26) is selected to calculate the stress intensity factor. Rearranging this equation so that the dimensionless crack opening displacements can be used leads to

$$\frac{E}{\sigma_o} C_I K_J = \frac{\left.\frac{Ev}{\sigma_o a}\right|_{y=0}}{\sqrt{\frac{R}{a}}} \tag{28}$$

where

$$C_I = \frac{4(1-\nu^2)}{E\sqrt{2\pi a}} \tag{29}$$

A plot of equation (28) as $\sqrt{R/a} \to 0$ can then be used to calculate K_I. Since the crack opening displacement is a function of the thickness variable, the previous stress intensity factor varies in the z-direction. However, if we were to account for the nonplane

strain conditions near the surface by using equation (27) or a corrected equation (26) for the definition of K_I, the stress intensity factor would become a constant across the thickness of the bar by definition. This approach would then result in a continuously varying definition of K_I across the thickness. It should be noted that the previous description of K_I is completely arbitrary and that it is questionable if it has any real significance in three-dimensional elasticity problems. However, values of K_I are still presented so that a comparison is possible between the calculated results and the published plane strain solutions (ref. 1).

Figures 12 and 14 show the calculation of the opening mode stress intensity factors from the plane strain crack opening displacements. Their variation across the thickness of the bar is shown in figures 13 and 15 for the two problems discussed in this report. Note that for the center-cracked bar K_I is maximum at the surface and minimum near the center. The value of K_I for the double-edge-crack specimen is independent of the $\tilde{z}$-coordinate since the crack opening displacement is constant across the thickness.

Although the stress intensity factors for these problems could be determined with reasonable accuracy, the associated type of singularities are difficult to evaluate because values of the normal stresses are needed within a distance of 0.05a or less from the crack edge. With the equal spacing of lines used in these examples, the minimum node location for these problems is about 0.06a. For this range of crack edge distance R, the singularity of the stresses is not defined.

Lewis Research Center,
National Aeronautics and Space Administration,
and
U.S. Army Air Mobility R&D Laboratory,
Cleveland, Ohio, January 4, 1973,
501-21.

APPENDIX A

SOLUTION OF THE SYSTEMS OF ORDINARY DIFFERENTIAL EQUATIONS WITH CONSTANT COEFFICIENTS

For the solution of equations (14) the following new variables are introduced:

$$\left.\begin{aligned} U_1 &= \tilde{u}_1 \\ U_2 = \tilde{u}_2 \;\ldots\; U_l &= \tilde{u}_l \\ U_{l+1} &= \frac{d\tilde{u}_1}{d\tilde{x}} \\ U_{l+2} = \frac{d\tilde{u}_2}{d\tilde{x}} \;\ldots\; U_{2l} &= \frac{d\tilde{u}_l}{d\tilde{x}} \end{aligned}\right\} \tag{A1}$$

In terms of these new variables, equations (14) can be written as a set of twice as many first-order differential equations. Hence, we have

$$\underset{2l\times 1}{\frac{d}{d\tilde{x}}\,U} = \underset{2l\times 2l}{A}\;\underset{2l\times 1}{U} + \underset{2l\times 1}{\bar{r}(\tilde{x})} \tag{A2}$$

where

$$\underset{2l\times 2l}{A} = \begin{bmatrix} \underset{l\times l}{0} & \underset{l\times l}{I} \\ \underset{l\times l}{K_x} & \underset{l\times l}{0} \end{bmatrix} \tag{A3}$$

$$\underset{2l\times 1}{\bar{r}(\tilde{x})} = \begin{Bmatrix} \underset{l\times 1}{0} \\ \underset{l\times 1}{r(\tilde{x})} \end{Bmatrix} \tag{A4}$$

The solution of equation (A2) is well known and can be written as (ref. 14)

$$\underset{2l\times 1}{U(\tilde{x})} = \underset{2l\times 2l}{e^{A\tilde{x}}}\ \underset{2l\times 1}{U(\tilde{0})} + \underset{2l\times 2l}{e^{A\tilde{x}}} \int_0^{\tilde{x}} \underset{2l\times 2l}{e^{-A\eta}}\ \underset{2l\times 1}{\bar{r}(\eta)}\ d\eta \tag{A5}$$

where U(0) is an initial value vector whose evaluation from given boundary conditions is discussed in appendix B and $e^{A\tilde{x}}$ is a matrix series given by the following equation:

$$e^{A\tilde{x}} = I + \frac{A\tilde{x}}{1!} + \frac{A^2\tilde{x}^2}{2!} + \frac{A^3\tilde{x}^3}{3!} + \cdots \tag{A6}$$

In terms of the coefficient matrix K_x, equation (A6) yields

$$e^{A\tilde{x}} = \begin{bmatrix} \sum_{m=0}^{\infty} \frac{\tilde{x}^{2m}}{(2m)!} K_x^m & \sum_{m=0}^{\infty} \frac{\tilde{x}^{2m+1}}{(2m+1)!} K_x^m \\ \sum_{m=0}^{\infty} \frac{\tilde{x}^{2m+1}}{(2m+1)!} K_x^{m+1} & \sum_{m=0}^{\infty} \frac{\tilde{x}^{2m}}{(2m)!} K_x^m \end{bmatrix} \tag{A7}$$

$$\underset{2l\times 2l}{e^{A\tilde{x}}} = \begin{bmatrix} \underset{l\times l}{A_{11}(\tilde{x})} & \underset{l\times l}{A_{12}(\tilde{x})} \\ \underset{l\times l}{A_{21}(\tilde{x})} & \underset{l\times l}{A_{22}(\tilde{x})} \end{bmatrix} \tag{A8}$$

From equations (A7) and (A8) we note that

$$A_{11}(\tilde{x}) = A_{22}(\tilde{x}) = \cosh K_x^{1/2}\tilde{x} \tag{A9}$$

$$A_{12}(\tilde{x}) = K_x^{-1/2} \sinh K_x^{1/2}\tilde{x} \tag{A10}$$

$$A_{21}(\tilde{x}) = K_x A_{12}(\tilde{x}) \tag{A11}$$

where $K_x^{1/2}$ is a matrix whose square is equal to K_x. Noting that A_{11} and A_{22} are

even functions of $\tilde{x}$ while A_{12} and A_{21} are odd functions of $\tilde{x}$, the inverse of $e^{A\tilde{x}}$ becomes

$$e^{-A\tilde{x}} = \begin{bmatrix} A_{11}(\tilde{x}) & -A_{12}(\tilde{x}) \\ -A_{21}(\tilde{x}) & A_{22}(\tilde{x}) \end{bmatrix} \tag{A12}$$

Substituting equations (A8) and (A12) into the identity of $e^{A\tilde{x}} \cdot e^{-A\tilde{x}} = I$ yields

$$\underset{l\times l}{A_{11}^2(\tilde{x})} - \underset{l\times l}{K_x}\underset{l\times l}{A_{12}^2(\tilde{x})} = \underset{l\times l}{I} \tag{A13}$$

Matrix functions (A9) and (A10) may be evaluated for each value of the independent variable from the series definitions given in equation (A7). However, for increasing values of $\tilde{x}$ serious convergence difficulties may arise and impractically large number of terms must be calculated. To avoid these computational difficulties, additive formulas for these matrix functions may be obtained from using the identity

$$e^{A\tilde{x}_1} \cdot e^{A\tilde{x}_2} = e^{A(\tilde{x}_1+\tilde{x}_2)}$$

In terms of the submatrices A_{ij} this identity yields the following two equations:

$$A_{11}(\tilde{x}_1 + \tilde{x}_2) = A_{11}(\tilde{x}_1)A_{11}(\tilde{x}_2) + K_x A_{12}(\tilde{x}_1)A_{12}(\tilde{x}_2) \tag{A14}$$

and

$$A_{12}(\tilde{x}_1 + \tilde{x}_2) = A_{12}(\tilde{x}_1)A_{11}(\tilde{x}_2) + A_{11}(\tilde{x}_1)A_{12}(\tilde{x}_2) \tag{A15}$$

Using equations (A7) in conjunction with equations (A14) and (A15) does not require the solution of an eigenvalue problem. However, greater accuracy is obtained if we consider the similarity transformation of

$$\underset{l\times l}{\Lambda} = \underset{l\times l}{P^{-1}}\,\underset{l\times l}{K_x}\,\underset{l\times l}{P} \tag{A16}$$

where Λ is a diagonal matrix whose elements are the eigenvalues of K_x. Appendix C

gives the details of the development showing how the eigenvalues and eigenvectors of a matrix having the form of K_x can be analytically evaluated. The eigenvalues of K_x are given by

$$\bar{\lambda}_{ij} = 2k_3\left[1 - \cos\left(\frac{i - 1}{NZ - 1}\right)\pi\right] + 2k_2\left[1 - \cos\left(\frac{j - 1}{NY - 1}\right)\pi\right] \tag{A17}$$

where $i = 1, 2, \ldots, NZ$, $j = 1, 2, \ldots, NY$, and k_2 and k_3 are constants given in appendix C. Note that these eigenvalues are ordered by fixing i first and then varying j.

The modal matrix or the matrix of eigenvectors corresponding to the previously ordered eigenvalues is given by

$$\underset{l\times l}{P} = \underset{NZ\times NZ}{P_2} \otimes \underset{NY\times NY}{P_1} \tag{A18}$$

where $\otimes$ denotes the Kroenecker product of two component modal matrices (ref. 16) whose elements are given by

$$P_{1_{sj}} = \cos\frac{(s - 1)(j - 1)}{NY - 1}\pi \qquad s, j = 1, 2, \ldots, NY \tag{A19}$$

$$P_{2_{ri}} = \cos\frac{(r - 1)(i - 1)}{NZ - 1}\pi \qquad r, i = 1, 2, \ldots, NZ \tag{A20}$$

The matrix functions (A9) and (A10) can now be evaluated in diagonalized form and retransformed according to the transformation

$$A_{11} = P\Lambda_{11}P^{-1} \tag{A21}$$

$$A_{12} = P\Lambda_{12}P^{-1} \tag{A22}$$

Note that the inverse of the modal matrix P can also be evaluated in closed form and the details of the derivations are shown in appendix C.

In the explicit evaluation of equation (A5), the value of the particular integral cannot be obtained until the vector $\bar{r}(\eta)$ is known along the x-directional lines. We define column vectors $B_1(\tilde{x})$ and $B_2(\tilde{x})$ as follows:

$$\underset{2\ell\times 1}{\begin{Bmatrix} B_1(\tilde{x}) \\ B_2(\tilde{x}) \end{Bmatrix}} = \underset{2\ell\times 2\ell}{\int_0^{\tilde{x}} e^{-A\eta}} \underset{2\ell\times 1}{\bar{r}(\eta)}\, d\eta \tag{A23}$$

In terms of the partitioned matrix functions, the integral in equation (A23) becomes

$$B_1(\tilde{x}) = -\int_0^{\tilde{x}} A_{12}(\eta) r(\eta)\, d\eta \tag{A24}$$

$$B_2(\tilde{x}) = \int_0^{\tilde{x}} A_{11}(\eta) r(\eta)\, d\eta \tag{A25}$$

If it is assumed that $r(\eta)$ is known, the particular integrals (eqs. (A24) and (A25)) can be evaluated. Using the partitioned form of the matrices we can write equation (A5) as

$$\begin{Bmatrix} \tilde{u}(\tilde{x}) \\ \dot{\tilde{u}}(\tilde{x}) \end{Bmatrix} = \begin{bmatrix} A_{11}(\tilde{x}) & A_{12}(\tilde{x}) \\ A_{21}(\tilde{x}) & A_{22}(\tilde{x}) \end{bmatrix} \left(\begin{Bmatrix} \tilde{u}(0) \\ \dot{\tilde{u}}(0) \end{Bmatrix} + \begin{Bmatrix} B_1(\tilde{x}) \\ B_2(\tilde{x}) \end{Bmatrix} \right) \tag{A26}$$

from which the solution vectors (17) and (22) can be directly constructed.

APPENDIX B

DEVELOPMENT OF INITIAL VALUE VECTORS

Since the problem in figure 2(a) is a two point boundary value problem, the initial values of both $\tilde{u}$ and $\dot{\tilde{u}}$ are usually not available. A method for evaluating the initial value vectors for equations (14) and (15) from given boundary conditions is now presented.

From symmetry conditions, we can immediately conclude that

$$\underset{\ell\times 1}{F_1} = \underset{\ell\times 1}{\tilde{u}(0)} = \underset{\ell\times 1}{0} \tag{B1}$$

The zero normal stress boundary condition on the face $\tilde{x} = \tilde{b}$ is used to evaluate the vector $\dot{\tilde{u}}(0)$. From equation (22) we have at $\tilde{x} = \tilde{b}$

$$\dot{\tilde{u}}(\tilde{b}) = A_{21}(\tilde{b})\left[\tilde{u}(0) + B_1(\tilde{b})\right] + A_{11}(\tilde{b})\left[\dot{\tilde{u}}(0) + B_2(\tilde{b})\right] \tag{B2}$$

Using equation (5) with the given normal stress boundary condition gives

$$\dot{\tilde{u}}(\tilde{b}) = \frac{-\nu}{1-\nu}\left(\dot{\tilde{v}} + \dot{\tilde{w}}\right)_{\tilde{x}=\tilde{b}} \tag{B3}$$

Provided $A_{11}(b)$ is not singular and using equations (B1) and (B3) we find from equation (B2) that

$$\underset{\ell\times 1}{F_2} = \underset{\ell\times 1}{\dot{\tilde{u}}(0)} = \frac{-\nu}{1-\nu}\underset{\ell\times\ell}{A_{11}^{-1}(\tilde{b})}\underset{\ell\times 1}{\left(\dot{\tilde{v}} + \dot{\tilde{w}}\right)_{\tilde{x}=\tilde{b}}} - \underset{\ell\times\ell}{A_{11}^{-1}(\tilde{b})}\underset{\ell\times\ell}{A_{21}(\tilde{b})}\underset{\ell\times 1}{B_1(\tilde{b})} - \underset{\ell\times 1}{B_2(\tilde{b})} \tag{B4}$$

Similar equations are obtained for the initial value vectors of equations (16) along the z-directional lines.

Along the y-directional lines the boundary conditions are somewhat more involved since in the crack plane mixed boundary conditions are specified. Denoting the number of y-directional lines falling over the crack surface as NIC and those falling outside as NOC, the zero normal stress condition over the crack face and the symmetry condition in the crack plane result in the following equations:

$$\underset{\text{NIC}\times 1}{\dot{\tilde{v}}(0)} = \frac{-\nu}{1-\nu}\left(\dot{\tilde{u}} + \dot{\tilde{w}}\right)_{\tilde{y}=0} \quad \text{inside crack} \tag{B5}$$

$$\underset{NOC\times 1}{\tilde{v}(0)} = (0)_{\substack{\tilde{y}=0 \\ \text{outside crack}}} \tag{B6}$$

If we assume that on the face $\tilde{y} = \tilde{L}$ there is a uniform stress of σ_o as shown in figure 2(a), the normal stress boundary condition on this face gives

$$\underset{m\times 1}{\dot{\tilde{v}}(L)} = \frac{\sigma_o}{E}\underset{m\times 1}{\frac{(1+\nu)(1-2\nu)}{(1-\nu)}} - \frac{\nu}{1-\nu}\left(\underset{m\times 1}{\dot{\tilde{u}}} + \underset{m\times 1}{\dot{\tilde{w}}}\right)_{\tilde{y}=\tilde{L}} \tag{B7}$$

This vector can be suitably partitioned into vectors $\underset{NIC\times 1}{\dot{\tilde{v}}_\alpha(\tilde{L})}$ and $\underset{NOC\times 1}{\dot{\tilde{v}}_\beta(\tilde{L})}$. For convenience of matrix manipulations, the following vectors are constructed:

$$\underset{2m\times 1}{\{V(0)\}} = \begin{Bmatrix} \underset{m\times 1}{\tilde{v}(0)} \\ \underset{m\times 1}{\dot{\tilde{v}}(0)} \end{Bmatrix} = \begin{Bmatrix} \underset{m\times 1}{F_3} \\ \underset{m\times 1}{F_4} \end{Bmatrix} = \begin{Bmatrix} \underset{NIC\times 1}{F_{3\alpha}} \\ \underset{NOC\times 1}{F_{3\beta}} \\ \underset{NIC\times 1}{F_{4\alpha}} \\ \underset{NOC\times 1}{F_{4\beta}} \end{Bmatrix} \tag{B8}$$

For the central-crack problem, values of $F_{4\alpha}$ and $F_{3\beta}$ are given by equations (B5) and (B6), respectively. An analogous solution to equation (A26) along the y-directional lines can be written as

$$\begin{Bmatrix} \tilde{v}(\tilde{y}) \\ \dot{\tilde{v}}(\tilde{y}) \end{Bmatrix} = \begin{bmatrix} D_{11}(\tilde{y}) & D_{12}(\tilde{y}) \\ D_{21}(\tilde{y}) & D_{22}(\tilde{y}) \end{bmatrix} \left(\begin{Bmatrix} \tilde{v}(0) \\ \dot{\tilde{v}}(0) \end{Bmatrix} + \begin{Bmatrix} B_3(\tilde{y}) \\ B_4(\tilde{y}) \end{Bmatrix} \right) \tag{B9}$$

From equation (B9), we can express $\dot{\tilde{v}}(\tilde{L})$ in a partitioned form consistent with equation (B8) as

$$\underset{NIC\times 1}{\left\{\begin{matrix}\tilde{\dot{v}}_\alpha\end{matrix}\right\}}_{\tilde{y}=\tilde{L}} = \underset{NIC\times NIC \quad NIC\times NOC}{\left[\begin{matrix}D_{21\alpha 1} & D_{21\alpha 2}\end{matrix}\right]}_{\tilde{y}=\tilde{L}} \left(\underset{NIC\times 1}{\left\{\begin{matrix}F_{3\alpha}\end{matrix}\right\}} + \underset{NIC\times 1}{\left\{\begin{matrix}B_{3\alpha}\end{matrix}\right\}}_{\tilde{y}=\tilde{L}} \right)$$

$$+ \underset{NIC\times NIC \quad NIC\times NOC}{\left[\begin{matrix}D_{22\alpha 1} & D_{22\alpha 2}\end{matrix}\right]}_{\tilde{y}=\tilde{L}} \left(\underset{NIC\times 1}{\left\{\begin{matrix}F_{4\alpha}\end{matrix}\right\}} + \underset{NIC\times 1}{\left\{\begin{matrix}B_{4\alpha}\end{matrix}\right\}}_{\tilde{y}=\tilde{L}} \right) \qquad \text{(B10)}$$

Equation (B10) leads to two matrix equations involving the two unknown vectors $F_{3\alpha}$ and $F_{4\beta}$. The solution of these equations yields

$$\underset{NOC\times 1}{F_{4\beta}} = \underset{NOC\times NOC}{D_a^{-1}} \underset{NOC\times 1}{\tilde{\dot{v}}_\beta}\Big|_{\tilde{y}=\tilde{L}} - \underset{NOC\times NOC}{D_a^{-1}} \underset{NOC\times NIC}{D_{21\beta 1}}\Big|_{\tilde{y}=\tilde{L}} \underset{NIC\times NIC}{D_{21\alpha 1}^{-1}}\Big|_{\tilde{y}=\tilde{L}} \underset{NIC\times 1}{\tilde{\dot{v}}_\alpha}\Big|_{\tilde{y}=\tilde{L}}$$

$$- \underset{NOC\times 1}{B_{4\beta}}\Big|_{\tilde{y}=\tilde{L}} - \underset{NOC\times NOC}{D_a^{-1}} \underset{NOC\times NOC}{D_b} \underset{NOC\times 1}{B_{3\beta}}\Big|_{\tilde{y}=\tilde{L}}$$

$$- \underset{NOC\times NOC}{D_a^{-1}} \underset{NOC\times NIC}{D_c} \left(\underset{NIC\times 1}{F_{4\alpha}} + \underset{NIC\times 1}{B_{4\alpha}}\Big|_{\tilde{y}=\tilde{L}} \right) \qquad \text{(B11)}$$

where

$$\underset{NOC\times NOC}{D_a} = \left(\underset{NOC\times NOC}{D_{22\beta 2}} - \underset{NOC\times NIC}{D_{21\beta 1}} \underset{NIC\times NIC}{D_{21\alpha 1}^{-1}} \underset{NIC\times NOC}{D_{22\alpha 2}} \right)_{\tilde{y}=\tilde{L}} \qquad \text{(B12)}$$

$$D_b = \left(D_{21\beta 2} - D_{21\beta 1} \; D_{21\alpha 1}^{-1} \; D_{21\alpha 2}\right)_{\tilde{y}=\tilde{L}} \tag{B13}$$

NOC×NOC NOC×NOC NOC×NIC NIC×NIC NIC×NOC

$$D_c = \left(D_{22\beta 1} - D_{21\beta 1} \; D_{21\alpha 1}^{-1} \; D_{22\alpha 1}\right)_{\tilde{y}=\tilde{L}} \tag{B14}$$

NOC×NIC NOC×NIC NOC×NIC NIC×NIC NIC×NIC

$$F_{3\alpha} = D_{21\alpha 1}^{-1}\Big|_{\tilde{y}=\tilde{L}} \dot{\tilde{v}}_\alpha\Big|_{\tilde{y}=\tilde{L}} - D_{21\alpha 1}^{-1}\Big|_{\tilde{y}=\tilde{L}} D_{21\alpha 2}\Big|_{\tilde{y}=\tilde{L}} B_{3\beta}\Big|_{\tilde{y}=\tilde{L}} - B_{3\alpha}\Big|_{\tilde{y}=\tilde{L}}$$

NIC×1 NIC×NIC NIC×1 NIC×NIC NIC×NOC NOC×1 NIC×1

$$- D_{21\alpha 1}^{-1}\Big|_{\tilde{y}=\tilde{L}} D_{22\alpha 1}\Big|_{\tilde{y}=\tilde{L}} \left(F_{4\alpha} + B_{4\alpha}\Big|_{\tilde{y}=\tilde{L}}\right)$$

NIC×NIC NIC×NIC NIC×1 NIC×1

$$- D_{21\alpha 1}^{-1}\Big|_{\tilde{y}=\tilde{L}} D_{22\alpha 2}\Big|_{\tilde{y}=\tilde{L}} \left(F_{4\beta} + B_{4\beta}\Big|_{\tilde{y}=\tilde{L}}\right)$$

NIC×NIC NIC×NOC NOC×1 NOC×1

(B15)

with $F_{4\beta}$ given by equation (B11). Note that although the full matrix $D_{21}\Big|_{\tilde{y}=\tilde{L}}$ is singular, the partitioned submatrices are not. Equations (B11) and (B15) together with the given boundary data completely specify the initial value vector needed for the solution of equations (15).

APPENDIX C

EVALUATION OF THE COEFFICIENT MATRIX EIGENVALUES AND EIGENVECTORS

For the x-directional lines shown in figure 1(a), the nondimensionalized coefficient matrix K_x can be arranged as

$$K_{x\ l\times l} = \begin{bmatrix} \underset{NY\times NY}{K_{x1}} & \underset{NY\times NY}{2K_{x2}} & 0 & 0 & 0 \\ \underset{NY\times NY}{K_{x2}} & \underset{NY\times NY}{K_{x1}} & \underset{NY\times NY}{K_{x2}} & 0 & 0 \\ 0 & \ddots & \ddots & \ddots & 0 \\ 0 & 0 & \underset{NY\times NY}{K_{x2}} & \underset{NY\times NY}{K_{x1}} & \underset{NY\times NY}{K_{x2}} \\ 0 & 0 & 0 & \underset{NY\times NY}{2K_{x2}} & \underset{NY\times NY}{K_{x1}} \end{bmatrix} \tag{C1}$$

where the submatrices K_{x1}, K_{x2}, and their elements k_1, k_2, and k_3 are

$$\left.\begin{aligned} k_1 &= 2(k_2 + k_3) \\ k_2 &= \frac{(1 - 2\nu)}{2(1 - \nu)}\left(\frac{1}{\tilde{h}_y^2}\right) \\ k_3 &= \frac{(1 - 2\nu)}{2(1 - \nu)}\left(\frac{1}{\tilde{h}_z^2}\right) \end{aligned}\right\} \tag{C2}$$

$$K_{x1}_{NY\times NY} = \begin{bmatrix} k_1 & -2k_2 & 0 & 0 & 0 \\ -k_2 & k_1 & -k_2 & 0 & 0 \\ 0 & \ddots & \ddots & \ddots & 0 \\ 0 & 0 & -k_2 & k_1 & -k_2 \\ 0 & 0 & 0 & -2k_2 & k_1 \end{bmatrix} \tag{C3}$$

$$K_{x2}_{NY\times NY} = \begin{bmatrix} -k_3 & 0 & 0 & 0 & 0 \\ 0 & -k_3 & 0 & 0 & 0 \\ 0 & 0 & \ddots & 0 & 0 \\ 0 & 0 & 0 & -k_3 & 0 \\ 0 & 0 & 0 & 0 & -k_3 \end{bmatrix} \tag{C4}$$

A close investigation of equation (C1) shows that the coefficient matrix K_x can be decomposed into component matrices having the following tridiagonal format:

$$\begin{bmatrix} 2 & -2 & 0 & 0 & 0 \\ -1 & 2 & -1 & 0 & 0 \\ 0 & \ddots & \ddots & \ddots & 0 \\ 0 & 0 & -1 & 2 & -1 \\ 0 & 0 & 0 & -2 & 2 \end{bmatrix} \tag{C5}$$

$M\times M$

The eigenvalues and eigenvectors of this type of matrix can then be obtained in closed

form. Noting that in equation (C1) we have NZ rows of submatrices each of order NY, we express the coefficient matrix as

$$\underset{l\times l}{K_x} = k_2 \underset{NZ\times NZ}{I_1} \otimes \underset{NY\times NY}{K_1} + k_3 \underset{NZ\times NZ}{K_2} \otimes \underset{NY\times NY}{I_2} \tag{C6}$$

where $\otimes$ denotes the Kroenecker product of two matrices (ref. 15). Matrices K_1 and K_2 have the desired form of matrix (C5) but are of different order. Associated with the matrices K_1 and K_2 are the following two eigenvalue problems:

$$\underset{NY\times NY}{K_1} \underset{NY\times 1}{X1} = \mu \underset{NY\times 1}{X1} \tag{C7}$$

$$\underset{NZ\times NZ}{K_2} \underset{NZ\times 1}{X2} = \delta \underset{NZ\times 1}{X2} \tag{C8}$$

where μ_j, $j = 1, 2, \ldots, NY$ denote the eigenvalues of K_1 and δ_i, $i = 1, 2, \ldots, NZ$ represent the eigenvalues of K_2. The original eigenvalue problem associated with the coefficient matrix K_x can be written as

$$\underset{l\times l}{K_x} \underset{l\times 1}{X3} = \bar{\lambda} \underset{l\times 1}{X3} \tag{C9}$$

After some matrix manipulations involving Kroenecker products (ref. 15), it can be shown that the eigenvalues $\bar{\lambda}_{ij}$ and the corresponding matrix of eigenvectors $X3^{ij}$ can be expressed in terms of the component matrix eigenvalues and eigenvectors. The results of these manipulations are

$$\bar{\lambda}_{ij} = k_3\delta_i + k_2\mu_j \tag{C10}$$

$$\underset{l\times l}{X3^{ij}} = \underset{NZ\times NZ}{X2^i} \otimes \underset{NY\times NY}{X1^j} \tag{C11}$$

where $i = 1, 2, \ldots, NZ$ and $j = 1, 2, \ldots, NY$. Equations (C10) and (C11) reduce the problem of equation (C9) to that of finding the eigenvalues and eigenvectors of matrix (C5).

The eigenvalues of the tridiagonal matrix (C5) can be obtained by using difference equation theory. The details of this method for finding the eigenvalues of matrix (C5)

can be found in reference 8, but the results for the problem of equation (C7) are

$$\mu_j = 2\left[1 - \cos\left(\frac{j-1}{M-1}\right)\pi\right] \qquad \begin{matrix} j = 1, 2, \ldots, M \\ M = NY \end{matrix} \tag{C12}$$

Similarly, the eigenvalues of K_2 become

$$\delta_i = 2\left[1 - \cos\left(\frac{i-1}{M-1}\right)\pi\right] \qquad \begin{matrix} i = 1, 2, \ldots, M \\ M = NZ \end{matrix} \tag{C13}$$

Substituting equations (C12) and (C13) into equation (C10) leads to the results of equation (A17).

The details of finding the eigenvectors corresponding to equations (C12) and (C13) are also given in reference 8. The results of these manipulations are given by equations (A19) and (A20), respectively. Substituting these eigenvectors into equation (C11) leads to equation (A18) which gives the modal matrix of the coefficient matrix K_x.

The inverse of the modal matrix P can be obtained from

$$P^{-1} = P_2^{-1} \otimes P_1^{-1} \tag{C14}$$

provided that closed form inverses of P_1 and P_2 can be found. Since these two matrices are of the same type, it is sufficient to investigate the closed form inverse of P_1 only.

As the first step in developing the closed form inverse of P_1, we construct a diagonal matrix D_1 which transforms the nonsymmetric matrix K_1 into a symmetric matrix K_1^S. The form of this transformation is

$$D_1^{1/2} K_1 D_1^{-1/2} = K_1^S \tag{C15}$$

where by definition the square root of a diagonal matrix is also a diagonal matrix whose elements are the square roots of the elements in the original matrix. For the tridiagonal matrix K_1 of order M, the diagonal matrix D_1 is of the form

$$D_1 = \begin{bmatrix} 1/2 & 0 & 0 & 0 & 0 & 0 & 0 \\ 0 & 1 & 0 & 0 & 0 & 0 & 0 \\ 0 & 0 & 1 & 0 & 0 & 0 & 0 \\ & \cdot & \cdot & \cdot & \cdot & \cdot & \\ & \cdot & \cdot & \cdot & \cdot & \cdot & \\ & \cdot & \cdot & \cdot & \cdot & \cdot & \\ 0 & 0 & 0 & 0 & 1 & 0 & 0 \\ 0 & 0 & 0 & 0 & 0 & 1 & 0 \\ 0 & 0 & 0 & 0 & 0 & 0 & 1/2 \end{bmatrix} \qquad \text{(C16)}$$

$M \times M$

Associated with matrix K_1 is the similarity transformation of

$$K_1 P_1 = P_1 \Lambda_1 \qquad \text{(C17)}$$

which can be written as

$$K_1 D_1^{-1/2} D_1^{1/2} P_1 = P_1 \Lambda_1 \qquad \text{(C18)}$$

Premultiplying equation (C18) by $D_1^{1/2}$ gives

$$K_1^s \left(D_1^{1/2} P_1 \right) = \left(D_1^{1/2} P_1 \right) \Lambda_1 \qquad \text{(C19)}$$

Since K_1^s is a symmetric matrix, the transformation of equation (C19) is orthogonal and the columns of $(D_1^{1/2} P_1)$ must be orthogonal. For an orthogonal transformation it is known that

$$\left(D_1^{1/2} P_1 \right)^T \left(D_1^{1/2} P_1 \right) = D \qquad \text{(C20)}$$

where T denotes the transpose and D is a diagonal matrix. Since D_1 is a diagonal matrix, the first term in equation (C20) can be written as

$$\left(D_1^{1/2} P_1 \right)^T = P_1^T D_1^{1/2} \qquad \text{(C21)}$$

Using equation (C21) in equation (C20) yields

$$P_1^T D_1 P_1 = D \tag{C22}$$

Premultiplying this equation by D^{-1} gives

$$\left(D^{-1} P_1^T D_1\right) P_1 = I \tag{C23}$$

from which we find that

$$P_1^{-1} = D^{-1} P_1^T D_1 \tag{C24}$$

Equation (C24) requires the inverse of an unknown matrix D. However, from equation (C22) it can be shown that the matrix D always has the form

$$\underset{M\times M}{D} = \begin{bmatrix} M-1 & 0 & 0 & 0 & 0 \\ 0 & \frac{M-1}{2} & 0 & 0 & 0 \\ & \ddots & \ddots & \ddots & \\ 0 & 0 & 0 & \frac{M-1}{2} & 0 \\ 0 & 0 & 0 & 0 & M-1 \end{bmatrix} \tag{C25}$$

Comparing matrices (C25) and (C16) we can conclude that.

$$D = \frac{M-1}{2} D_1^{-1} \tag{C26}$$

Substituting this equation into equation (C24) gives the final closed form inverse of P_1 as

$$\underset{M\times M}{P_1^{-1}} = \frac{2}{M-1}\ \underset{M\times M}{D_1}\ \underset{M\times M}{P_1^T}\ \underset{M\times M}{D_1} \tag{C27}$$

A similar equation can be written for the inverse of the modal matrix P_2. With the closed form solution of the component modal matrices and their inverses, the diagonalized form of K_x is obtained from equation (A16).

REFERENCES

1. Paris, Paul C.; and Sih, George C.: Stress Analysis of Cracks. Fracture Toughness Testing and Its Applications. Spec. Tech. Publ. No. 381, ASTM, 1965, pp. 30-83.

2. Sneddon, I. N.: The Distribution of Stress in the Neighborhood of a Crack in an Elastic Solid. Proc. Roy. Soc. (London), Ser. A, vol. 187, no. 1009, Oct. 22, 1946, pp. 229-260.

3. Smith, Frederick W.: Stresses Near a Semi-Circular Edge Crack. Ph.D. Thesis, Univ. of Washington, 1966.

4. Kassir, M. K.; and Sih, G. C.: Three-Dimensional Stress Distribution Around an Elliptical Crack Under Arbitrary Loadings. J. Appl. Mech., vol. 33, no. 3, Sept. 1966, pp. 601-611.

5. Ayres, David J.: A Numerical Procedure for Calculating Stress and Deformation Near a Slit in a Three-Dimensional Elastic-Plastic Solid. NASA TM X-52440, 1968.

6. Cruse, T. A.; and Van Buren, W.: Three-Dimensional Elastic Stress Analysis of a Fracture Specimen with an Edge Crack. Int. J. Fracture Mech., vol. 7, Mar. 1971, pp. 1-15.

7. Hartranft, R. J.; and Sih, G. C.: The Use of Eigenfunction Expansions in the General Solution of Three-Dimensional Crack Problems. J. Math. Mech., vol. 19, no. 2, Aug. 1969, pp. 123-138.

8. Gyekenyesi, John P.: Solution of Some Mixed Boundary Value Problems of Three-Dimensional Elasticity by the Method of Lines. Ph.D. Thesis, Michigan State Univ., 1972.

9. Faddeva, V. N.: The Method of Lines Applied to Some Boundary Problems. Trudy Mat. Inst. Steklov., vol. 28, 1949, pp. 73-103.

10. Irobe, Makoto: Method of Numerical Analysis for Three-Dimensional Elastic Problems. Proceedings of the 16th Japan National Congress for Applied Mechanics. Central Scientific Publ., 1968, pp. 1-7.

11. Walker, George E., Jr.: A Study of the Applicability of the Method of Potential to Inclusions of Various Shapes in Two and Three-Dimensional Elastic and Thermoelastic Stress Fields. Ph.D. Thesis, Univ. of Washington, 1969.

12. Brown, W. F., Jr.; and Srawley, J. E.: Plane Strain Crack Toughness Testing of High Strength Metallic Materials. Spec. Tech. Publ. No. 410, ASTM, 1967.

13. Mendelson, Alexander; Gross, Benard; and Srawley, John E.: Evaluation of the Use of a Singularity Element in Finite-Element Analysis of Center-Cracked Plates. NASA TN D-6703, 1972.

14. Frazer, R. A.; Duncan, W. J.; and Collar, A. R.: Elementary Matrices and Some Applications to Dynamics and Differential Equations. Cambridge University Press, 1938.

15. Halmos, Paul R.: Finite-Dimensional Vector Spaces. Second ed., D. Van Nostrand, Co., Inc., 1958.

TABLE I. - DIMENSIONLESS x-DIRECTIONAL DISPLACEMENTS $Eu/\sigma_o a$ FOR RECTANGULAR BAR UNDER UNIFORM TENSION CONTAINING THROUGH-THICKNESS CENTRAL CRACK

[$\tilde{a} = 1.0$; $\tilde{b} = 2.0$; $\tilde{L} = 1.75$; $\tilde{t} = 1.5$ (48 by 96 by 128 x-, y-, z-directional lines, respectively).]

$\tilde{y}$	$\tilde{x}$						$\tilde{z}$
	0.00	0.40	0.80	1.20	1.60	2.00	
	x-Directional displacements, $Eu/\sigma_o a$						
0.00	0.000	-0.474	-0.828	-1.026	-1.095	-1.192	0.0
.50	↓	-.143	-.275	-.541	-.783	-.920	↓
1.0		-.025	-.092	-.242	-.420	-.565	
1.75		.169	.257	.238	.148	.029	
0.00	0.000	-0.479	-0.846	-1.00	-1.030	-1.105	0.9
.50	↓	-.119	-.244	-.498	-.742	-.888	↓
1.0		-.015	-.076	-.220	-.393	-.540	
1.75		.180	.276	.260	.163	.042	
0.00	0.000	-0.395	-0.713	-0.890	-0.991	-1.091	1.5
.50	↓	-.062	-.156	-.422	-.699	-.862	↓
1.0		.009	-.035	-.182	-.367	-.520	
1.75		.179	.278	.263	.168	.050	

TABLE II. - DIMENSIONLESS y-DIRECTIONAL DISPLACEMENTS $Ev/\sigma_o a$ FOR RECTANGULAR BAR UNDER UNIFORM TENSION CONTAINING THROUGH-THICKNESS CENTRAL CRACK

[$\tilde{a} = 1.0$; $\tilde{b} = 2.0$; $\tilde{L} = 1.75$; $\tilde{t} = 1.5$ (48 by 96 by 128 x-, y-, z-directional lines, respectively).]

$\tilde{z}$	$\tilde{y}$						$\tilde{x}$
	0.00	0.25	0.50	1.00	1.50	1.75	
	y-Directional displacements, $Ev/\sigma_o a$						
0.00	2.112	2.227	2.315	2.578	2.893	3.048	0.0
.60	2.197	2.322	2.415	2.638	2.952	3.107	↓
.90	2.218	2.334	2.420	2.638	2.956	3.117	
1.50	2.249	2.323	2.402	2.631	2.945	3.125	
0.00	1.252	1.354	1.552	2.014	2.453	2.660	0.8
.60	1.287	1.424	1.622	2.072	2.512	2.716	↓
.90	1.297	1.431	1.627	2.074	2.515	2.721	
1.50	1.313	1.411	1.591	2.029	2.471	2.686	
0.00	0.000	0.270	0.572	1.173	1.713	1.966	1.6
.60	↓	.288	.599	1.202	1.736	1.986	↓
.90		.291	.604	1.206	1.739	1.986	
1.50		.290	.589	1.179	1.716	1.965	
0.00	0.000	0.139	0.351	0.868	1.372	1.620	2.0
.60	↓	.174	.384	.883	1.385	1.630	↓
.90		.176	.388	.890	1.390	1.638	
1.50		.167	.377	.881	1.380	1.626	

TABLE III. - DIMENSIONLESS z-DIRECTIONAL DISPLACEMENTS $Ew/\sigma_o a$ FOR RECTANGULAR BAR UNDER UNIFORM TENSION CONTAINING THROUGH-THICKNESS CENTRAL CRACK

[$\tilde{a} = 1.0$; $\tilde{b} = 2.0$; $\tilde{L} = 1.75$; $\tilde{t} = 1.5$ (48 by 96 by 128 x-, y-, z-directional lines, respectively).]

$\tilde{x}$	$\tilde{z}$						$\tilde{y}$
	0.00	0.30	0.60	0.90	1.20	1.50	
	z-Directional displacements, $Ew/\sigma_o a$						
0.00	0.000	-0.008	-0.034	-0.053	-0.041	-0.025	0.0
.80	↓	-.054	-.128	-.205	-.266	-.267	↓
1.60	↓	-.105	-.225	-.355	-.492	-.628	↓
2.00	↓	-.119	-.237	-.356	-.465	-.554	↓
0.00	0.000	-0.048	-0.094	-0.134	-0.167	-0.194	0.5
.80	↓	-.078	-.156	-.234	-.309	-.377	↓
1.60	↓	-.110	-.223	-.340	-.458	-.657	↓
2.00	↓	-.117	-.231	-.343	-.451	-.549	↓
0.00	0.000	-0.080	-0.160	-0.241	-0.324	-0.408	1.0
.80	↓	-.093	-.185	-.278	-.374	-.472	↓
1.60	↓	-.109	-.218	-.328	-.436	-.543	↓
2.00	↓	-.114	-.226	-.335	-.440	-.544	↓
0.00	0.000	-0.117	-0.224	-0.334	-0.461	-0.614	1.75
.80	↓	-.116	-.218	-.319	-.429	-.558	↓
1.60	↓	-.113	-.219	-.321	-.422	-.526	↓
2.00	↓	-.116	-.224	-.327	-.427	-.526	↓

TABLE IV. - DIMENSIONLESS x-DIRECTIONAL DISPLACEMENTS $Eu/\sigma_o a$ FOR RECTANGULAR BAR UNDER UNIFORM TENSION CONTAINING THROUGH-THICKNESS DOUBLE-EDGE CRACKS

[$\tilde{a} = 1.0$; $\tilde{b} = 2.0$; $\tilde{L} = 1.75$; $\tilde{t} = 1.5$ (48 by 96 by 128 x-, y-, z-directional lines, respectively).]

$\tilde{y}$	$\tilde{x}$						$\tilde{z}$
	0.00	0.40	0.80	1.20	1.60	2.00	
	x-Directional displacements, $Eu/\sigma_o a$						
0.00	0.000	0.389	0.817	1.092	1.218	1.268	0.0
.50	↓	.054	-.018	-.128	-.082	-.054	↓
1.00	↓	-.224	-.478	-.700	-.852	-.946	↓
1.75	↓	-.646	-1.231	-1.688	-1.989	-2.181	↓
0.00	0.000	0.348	0.784	1.078	1.152	1.169	0.9
.50	↓	.030	-.060	-.187	-.158	-.133	↓
1.00	↓	-.256	-.537	-.784	-.924	-.999	↓
1.75	↓	-.683	-1.295	-1.766	-2.066	-2.261	↓
0.00	0.000	0.292	0.599	0.831	0.911	0.941	1.5
.50	↓	-.028	-.196	-.374	-.344	-.314	↓
1.00	↓	-.293	-.616	-.892	-1.038	-1.113	↓
1.75	↓	-.693	-1.317	-1.801	-2.106	-2.291	↓

TABLE V. - DIMENSIONLESS y-DIRECTIONAL DISPLACEMENTS $Ev/\sigma_0 a$ FOR RECTANGULAR BAR UNDER UNIFORM TENSION CONTAINING THROUGH-THICKNESS DOUBLE-EDGE CRACKS

[$\tilde{a} = 1.0$; $\tilde{b} = 2.0$; $\tilde{L} = 1.75$; $\tilde{t} = 1.5$ (48 by 96 by 128 x-, y-, z-directional lines, respectively).]

$\tilde{z}$	$\tilde{y}$						$\tilde{x}$
	0.00	0.25	0.50	1.00	1.50	1.75	
	y-Directional displacements, $Ev/\sigma_0 a$						
0.00	0.000	0.258	0.549	1.238	1.879	2.264	0.0
.60	↓	.222	.493	1.146	1.856	2.249	↓
.90	↓	.228	.503	1.159	1.869	2.257	↓
1.50	↓	.248	.529	1.182	1.907	2.277	↓
0.00	0.000	0.588	1.081	1.916	2.474	2.850	0.8
.60	↓	.509	1.011	1.825	2.521	2.878	↓
.90	↓	.520	1.025	1.840	2.536	2.891	↓
1.50	↓	.601	1.086	1.874	2.587	2.931	↓
0.00	3.374	3.432	3.500	3.785	4.036	4.305	1.6
.60	3.369	3.393	3.442	3.698	4.131	4.387	↓
.90	3.370	3.390	3.440	3.700	4.139	4.403	↓
1.50	3.412	3.460	3.497	3.721	4.161	4.428	↓
0.00	4.547	4.536	4.512	4.649	4.799	5.060	2.0
.60	4.515	4.498	4.463	4.546	4.938	5.186	↓
.90	4.512	4.491	4.453	4.538	4.941	5.198	↓
1.50	4.572	4.536	4.475	4.537	4.938	5.196	↓

TABLE VI. - DIMENSIONLESS z-DIRECTIONAL DISPLACEMENTS $Ew/\sigma_0 a$ FOR RECTANGULAR BAR UNDER UNIFORM TENSION CONTAINING THROUGH-THICKNESS DOUBLE-EDGE CRACKS

[$\tilde{a} = 1.0$; $\tilde{b} = 2.0$; $\tilde{L} = 1.75$; $\tilde{t} = 1.5$ (48 by 96 by 128 x-, y-, z-directional lines, respectively).]

$\tilde{x}$	$\tilde{z}$						$\tilde{y}$
	0.00	0.30	0.60	0.90	1.20	1.50	
	z-Directional displacements, $Ew/\sigma_0 a$						
0.00	0.000	-0.228	-0.436	-0.647	-0.871	-1.120	0.0
.80	↓	-.201	-.394	-.609	-.888	-1.288	↓
1.60	↓	-.100	-.179	-.238	-.274	-.293	↓
2.00	↓	-.059	-.102	-.123	-.123	-.119	↓
0.00	0.000	-0.189	-0.379	-0.566	-0.748	-0.928	0.5
.80	↓	-.167	-.337	-.513	-.702	-.888	↓
1.60	↓	-.090	-.172	-.249	-.317	-.375	↓
2.00	↓	-.052	-.110	-.164	-.205	-.219	↓
0.00	0.000	-0.134	-0.270	-0.400	-0.519	-0.625	1.0
.80	↓	-.118	-.241	-.363	-.479	-.584	↓
1.60	↓	-.057	-.137	-.222	-.301	-.370	↓
2.00	↓	-.038	-.097	-.165	-.231	-.287	↓
0.00	0.000	-0.095	-0.188	-0.267	-0.315	-0.308	1.75
.80	↓	-.097	-.186	-.264	-.323	-.343	↓
1.60	↓	-.081	-.149	-.221	-.297	-.374	↓
2.00	↓	-.067	-.123	-.190	-.270	-.361	↓

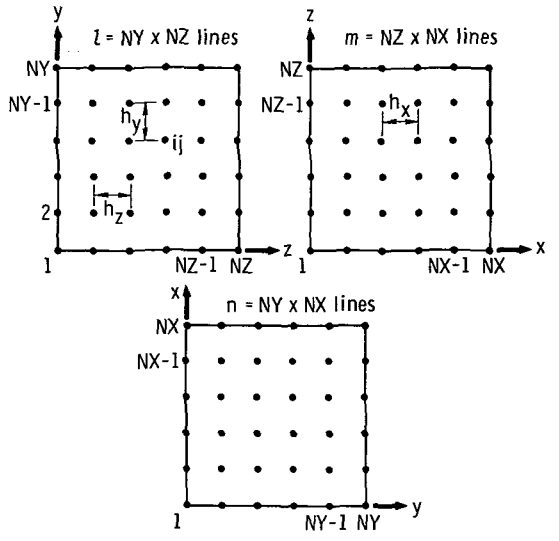

(a) Three sets of lines parallel to x-, y-, and z-coordinates and perpendicular to corresponding coordinate planes.

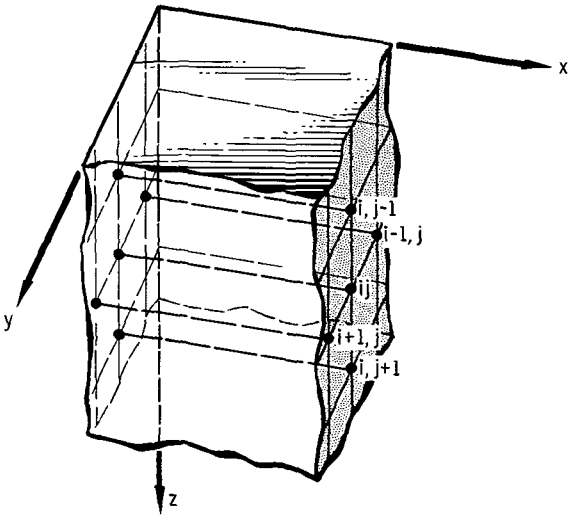

(b) Set of interior lines parallel to x-coordinate.

Figure 1. - Sets of lines parallel to Cartesian coordinates.

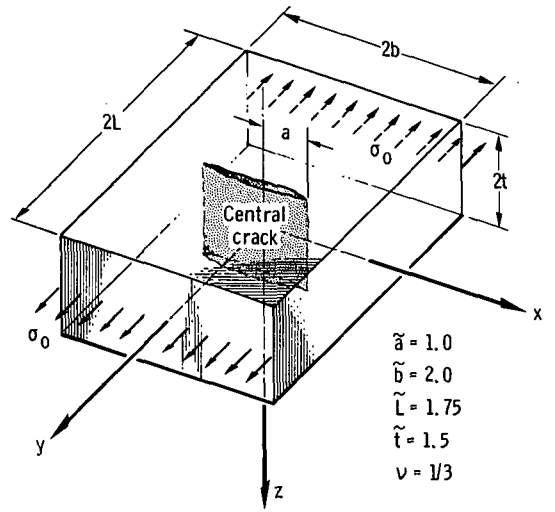

(a) Rectangular bar with through-thickness central crack.

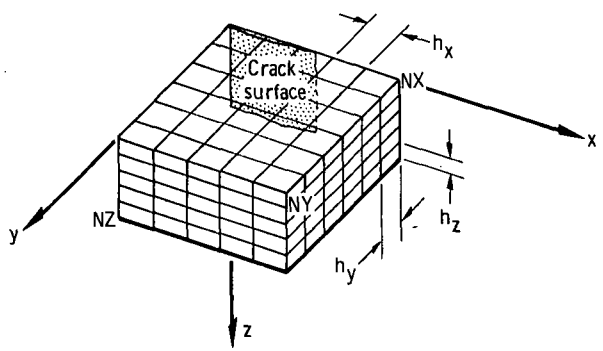

(b) Discretized region of rectangular bar with through-thickness central crack.

Figure 2. - Rectangular bar with through-thickness central crack under uniform tension.

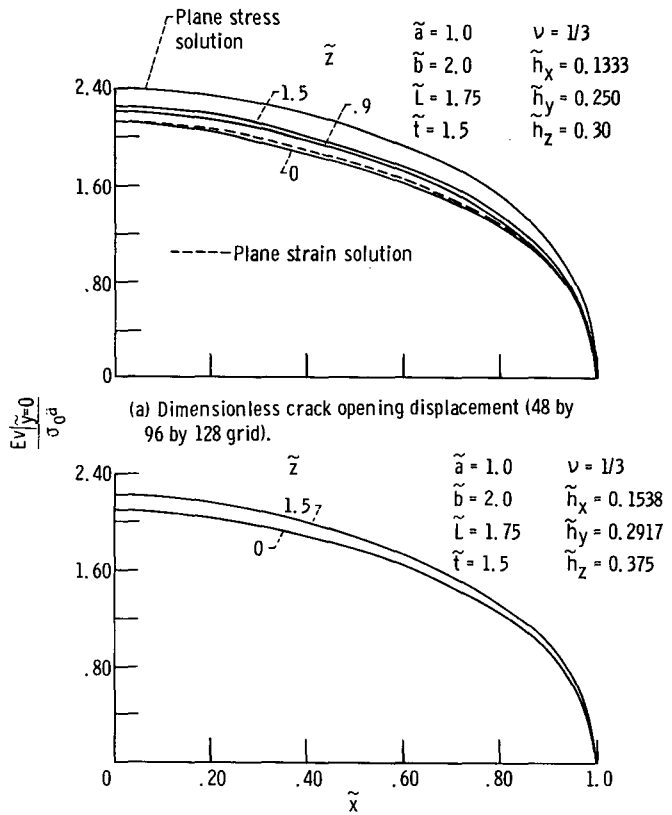

(a) Dimensionless crack opening displacement (48 by 96 by 128 grid).

(b) Dimensionless crack opening displacement (35 by 70 by 98 grid).

Figure 3. - Dimensionless crack opening displacement for rectangular bar under uniform tension containing through-thickness central crack.

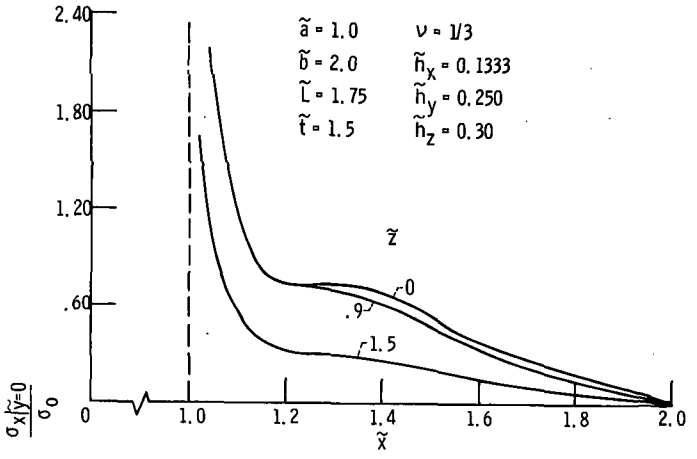

(a) Dimensionless x-directional normal stress as function of $\tilde{x}$.

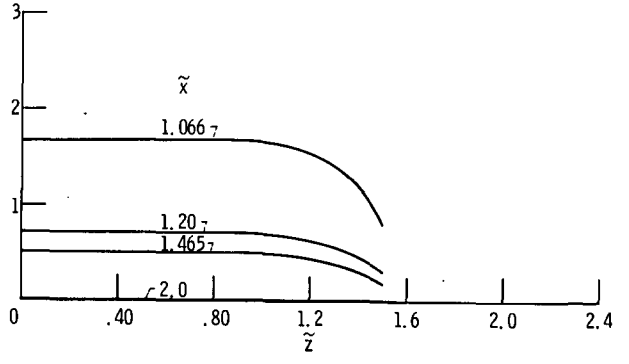

(b) Dimensionless x-directional normal stress as function of $\tilde{z}$.

Figure 4. - Dimensionless x-directional normal stress distribution in crack plane for rectangular bar under uniform tension containing through-thickness central crack.

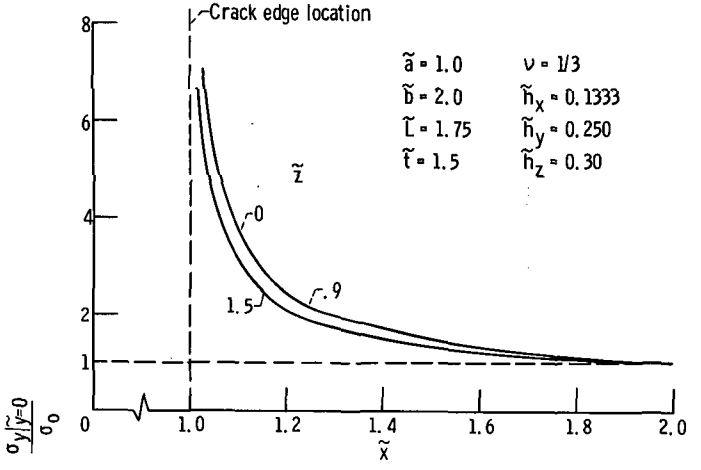

(a) Dimensionless y-directional normal stress as function of $\tilde{x}$.

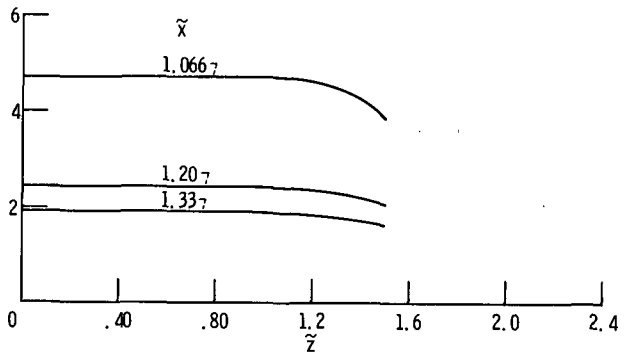

(b) Dimensionless y-directional normal stress as function of $\tilde{z}$.

Figure 5. - Dimensionless y-directional normal stress distribution in crack plane for rectangular bar under uniform tension containing through-thickness central crack.

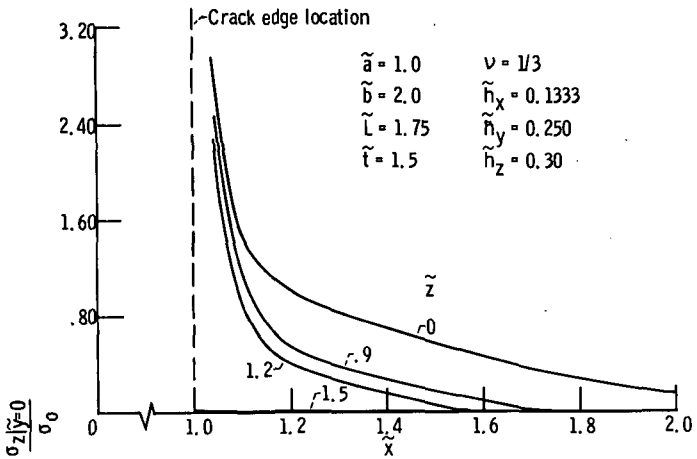

(a) Dimensionless z-directional normal stress as function of $\tilde{x}$.

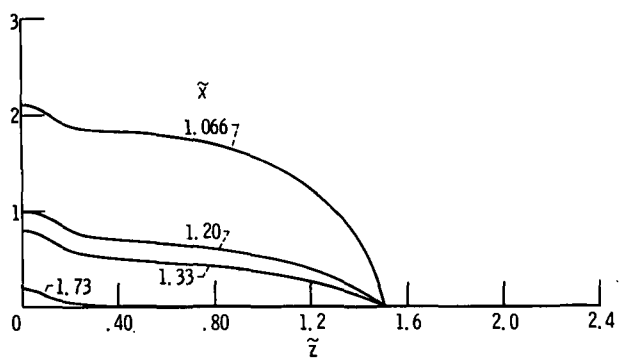

(b) Dimensionless z-directional normal stress as function of $\tilde{z}$.

Figure 6. - Dimensionless z-directional normal stress distribution in crack plane for rectangular bar under uniform tension containing through-thickness central crack.

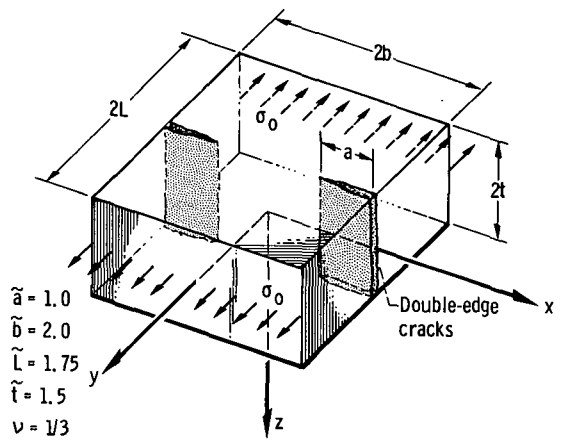

(a) Rectangular bar with through-thickness double-edge cracks.

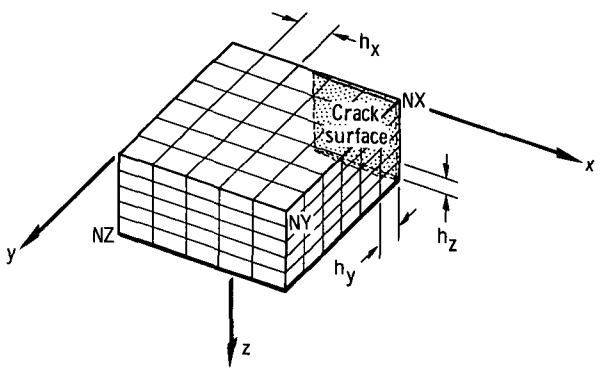

(b) Discretized region of rectangular bar with double-edge cracks.

Figure 7. - Rectangular bar with through-thickness double-edge cracks under uniform tension.

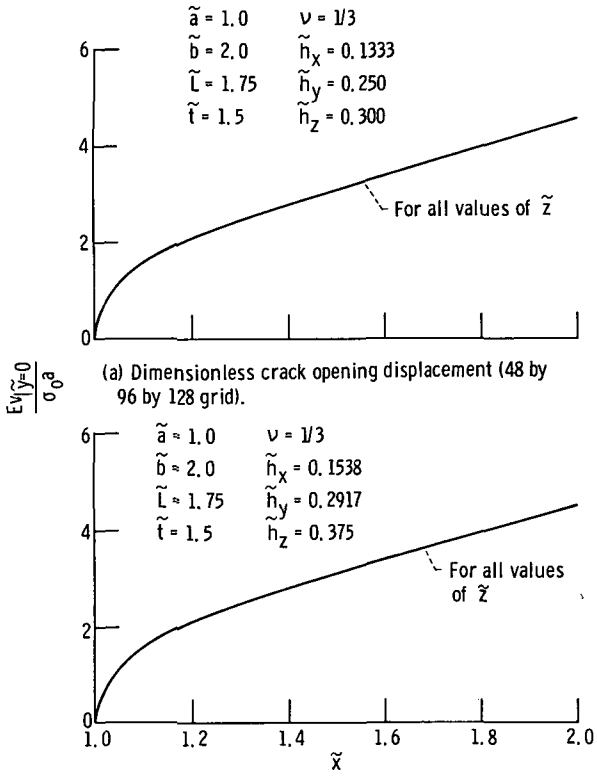

(a) Dimensionless crack opening displacement (48 by 96 by 128 grid).

(b) Dimensionless crack opening displacement (35 by 70 by 98 grid).

Figure 8. - Dimensionless crack opening displacement for rectangular bar under uniform tension containing through-thickness double-edge cracks.

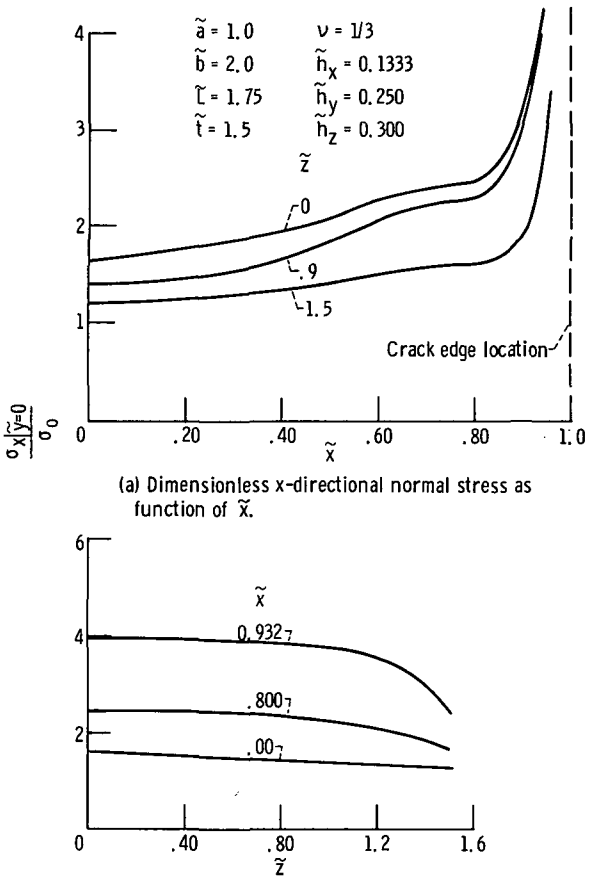

(a) Dimensionless x-directional normal stress as function of $\tilde{x}$.

(b) Dimensionless x-directional normal stress as function of $\tilde{z}$.

Figure 9. - Dimensionless x-directional normal stress distribution in crack plane for rectangular bar under uniform tension containing through-thickness double-edge cracks.

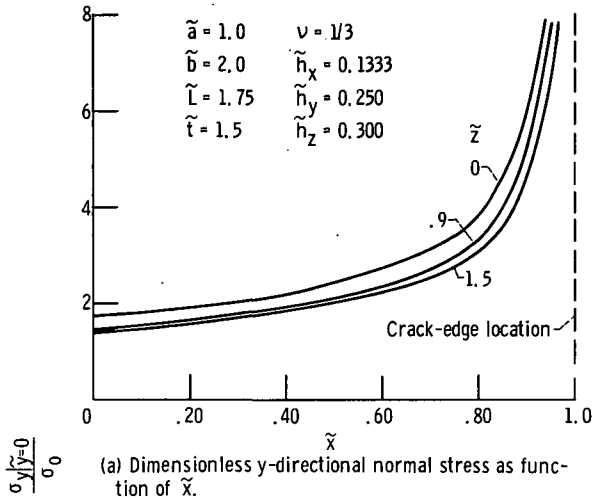

(a) Dimensionless y-directional normal stress as function of $\tilde{x}$.

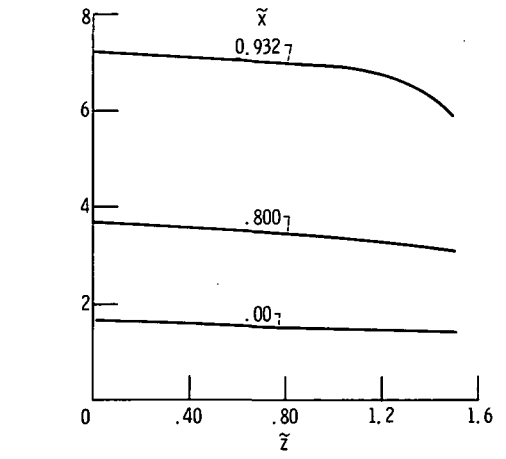

(b) Dimensionless y-directional normal stress as function of $\tilde{z}$.

Figure 10. - Dimensionless y-directional normal stress distribution in crack plane for rectangular bar under uniform tension containing through-thickness double-edge cracks.

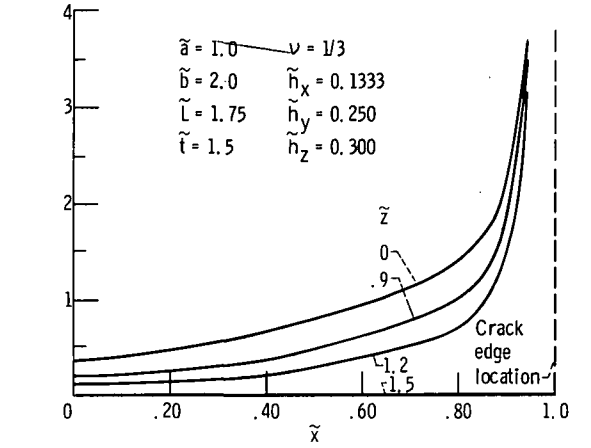

(a) Dimensionless z-directional normal stress as function of x.

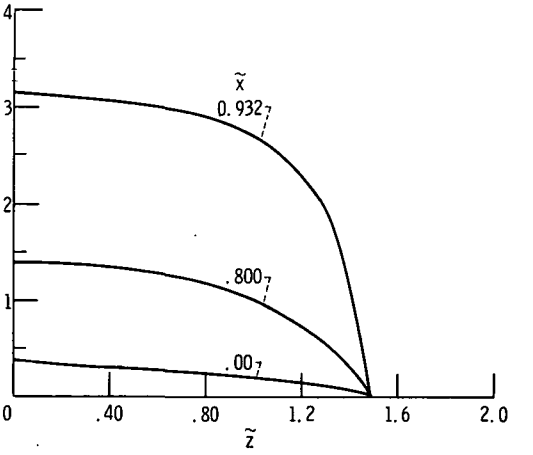

(b) Dimensionless z-directional normal stress as function of z.

Figure 11. - Dimensionless z-directional normal stress distribution in crack plane for rectangular bar under uniform tension containing through-thickness double-edge cracks.

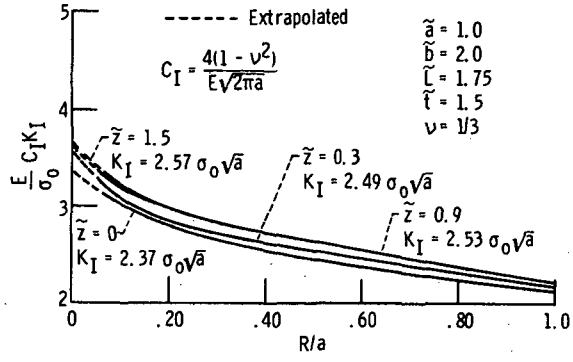

Figure 12. - Calculation of stress intensity factors K_I for rectangular bar under uniform tension containing through-thickness central crack.

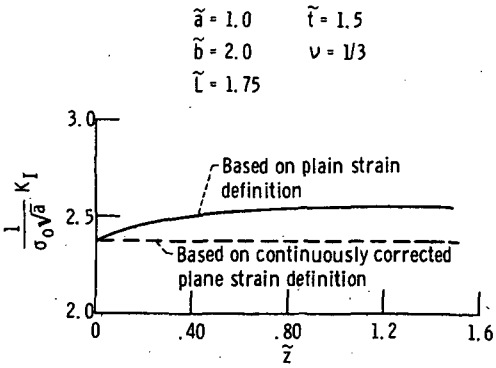

Figure 13. - Variation of stress intensity factor K_I across thickness for rectangular bar under uniform tension containing through-thickness central crack.

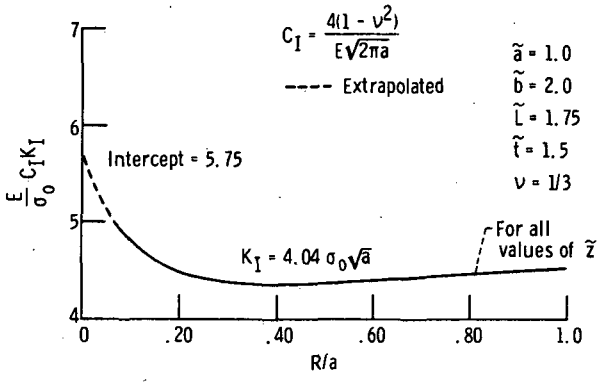

Figure 14. - Calculation of stress intensity factors K_I for rectangular bar under uniform tension containing through-thickness double-edge cracks.

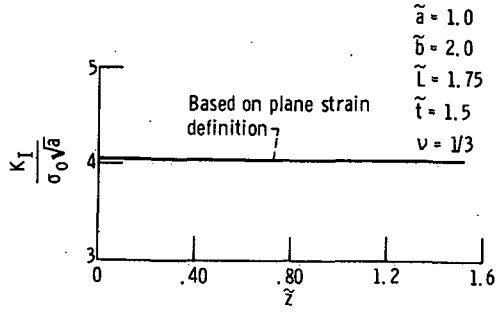

Figure 15. - Variation of stress intensity factor K_I across thickness for rectangular bar under uniform tension containing through-thickness double-edge cracks.

Page Intentionally Left Blank

NATIONAL AERONAUTICS AND SPACE ADMINISTRATION
WASHINGTON, D.C. 20546

OFFICIAL BUSINESS
PENALTY FOR PRIVATE USE $300

SPECIAL FOURTH-CLASS RATE BOOK

POSTAGE AND FEES PAID
NATIONAL AERONAUTICS AND SPACE ADMINISTRATION
451

U.S.MAIL

POSTMASTER: If Undeliverable (Section 158 Postal Manual) Do Not Return

"The aeronautical and space activities of the United States shall be conducted so as to contribute . . . to the expansion of human knowledge of phenomena in the atmosphere and space. The Administration shall provide for the widest practicable and appropriate dissemination of information concerning its activities and the results thereof."

—NATIONAL AERONAUTICS AND SPACE ACT OF 1958

NASA SCIENTIFIC AND TECHNICAL PUBLICATIONS

TECHNICAL REPORTS: Scientific and technical information considered important, complete, and a lasting contribution to existing knowledge.

TECHNICAL NOTES: Information less broad in scope but nevertheless of importance as a contribution to existing knowledge.

TECHNICAL MEMORANDUMS: Information receiving limited distribution because of preliminary data, security classification, or other reasons. Also includes conference proceedings with either limited or unlimited distribution.

CONTRACTOR REPORTS: Scientific and technical information generated under a NASA contract or grant and considered an important contribution to existing knowledge.

TECHNICAL TRANSLATIONS: Information published in a foreign language considered to merit NASA distribution in English.

SPECIAL PUBLICATIONS: Information derived from or of value to NASA activities. Publications include final reports of major projects, monographs, data compilations, handbooks, sourcebooks, and special bibliographies.

TECHNOLOGY UTILIZATION PUBLICATIONS: Information on technology used by NASA that may be of particular interest in commercial and other non-aerospace applications. Publications include Tech Briefs, Technology Utilization Reports and Technology Surveys.

Details on the availability of these publications may be obtained from:

SCIENTIFIC AND TECHNICAL INFORMATION OFFICE

NATIONAL AERONAUTICS AND SPACE ADMINISTRATION

Washington, D.C. 20546